

Structure and Evolution of Lithospheric Slab Beneath the Sunda Arc, Indonesia

Sri Widiyantoro* and Rob van der Hilst†

Tomographic imaging reveals seismic anomalies beneath the Sunda island arc, Indonesia, that suggest that the lithospheric slab penetrates to a depth of at least 1500 kilometers. The Sunda slab forms the eastern end of a deep anomaly associated with the past subduction of the plate underlying the Mesozoic Tethys Ocean. In accord with previous studies, the lithospheric slab was imaged as a continuous feature from the surface to the lower mantle below Java, with a local deflection where the slab continues into the lower mantle. The deep slab seems to be detached from the upper mantle slab beneath Sumatra. This complex slab structure is related to the Tertiary evolution of southeastern Asia and the Indian Ocean region.

The tectonic evolution of island arcs and lithospheric fragments in southeastern Asia is complex because of the interaction of several lithospheric plates (Fig. 1A) (1–3). Without sufficient land-based paleomagnetic measurements and information about the structure of the deep Earth, the relative plate motion in this complex plate boundary zone has often been reconstructed from data on ocean-floor spreading of the major oceanic plates using geometrical fits on a sphere (4). Seismic imaging provides information about Earth's interior structure that helps understanding of the geological history. Here, we focus on the northward subduction of the complex Indo-Australian Plate along the Sunda arc (from northwestern Sumatra, along Java, to Flores).

In the east, continental lithosphere (Australia) has been colliding with the Banda arc since about 5 million years ago (Ma), whereas further to the west, the oceanic part of the Indo-Australian Plate subducts beneath the Java trench. The age of the subducting ocean floor varies from 50 to 90 Ma along Sumatra to 100 to 135 Ma and 140 to 160 Ma near Java and Flores, respectively. The lateral variation of the nature and age of the subducting plate influences the style of deformation and seismicity along the Sunda arc (5). Earthquakes with focal depths of up to 670 km occur in the steeply dipping (~60°) seismic zone beneath the Java arc, but there is a seismic gap between depths of 350 and 500 km (6–8). Beneath Sumatra, the seismic zone dips ~30° to 45°, but there are no earthquakes deeper than 300 km, which has been attributed to the relatively young age of subducted lithosphere (8, 9).

We inferred from the tomographic im-

ages that the slab is continuous across the seismic gap beneath Java and that there is a pronounced seismic anomaly in the lower mantle. This is in good agreement with conclusions based on previous tomographic studies (10, 11), even though different data sets and reference Earth models were used, leaving little doubt that the deep Java slab is a realistic structural feature. In addition, we (i) present evidence for a lower mantle anomaly beneath Sumatra and for the detachment of the upper mantle slab from the deeper slab, (ii) explore the substantial lateral variation in slab morphology, and (iii) discuss the geological evolution of the lithospheric slab, which seems to be more complex than that of the western Pacific subduction zones (12, 13).

We investigated mantle structure beneath the Indonesian region (Fig. 1A) by means of tomographic images produced by linearized inversion of travel-time data of direct *P* phases and the surface-reflected depth phases *pP* and *pwP* (14, 15). The radially stratified *iasp91* model (16) was used as a global reference for the seismic velocities and for the tracing of the ray paths. The inclusion of the depth phases improved the sampling of mantle structure away from the seismic zones, in particular beneath the back arc regions (Fig. 1, A and B), and provided constraints on earthquake focal depth. The hypocenters and phase data used were derived from the reprocessing of the entire data catalog of the International Seismological Centre, which involved nonlinear hypocenter relocation and phase reidentification (17). This data set was augmented by data from the Australian *Skippy* project (18). We used about 1.3 million data, constituting a linear system of about 275,000 equations (19), from nearly 17,000 earthquakes within the study area recorded at one or more of over 2000 seismological stations worldwide. Following Fukao *et al.* (10), we inverted both regional and global structure simultaneously to minimize contamination of our regional model

Research School of Earth Sciences, Australian National University, Canberra, ACT 0200, Australia.

*On leave from the Department of Geophysics, Bandung Institute of Technology, Bandung 40132, Indonesia.

†Present address: Department of Earth, Atmospheric, and Planetary Sciences, Massachusetts Institute of Technology, Cambridge, MA 02139, USA.

50 fs, the integration step was set at 1.25 fs, and the momenta were randomized every 5 fs. For the next 150 fs, they were set at 2.5 fs and 10 fs. For the remaining 800 fs we used an integration step of 5 fs, with randomizations every 10 fs.

25. We ran 28 trajectories per case, representing a total simulation time of 9.52 ns, using 290 central processing unit (CPU) hours on an IBM/RS6000 model 590 computer (5.6 ns) and another 650 CPU hours on an Apple Power Macintosh 7100/82 computer (3.92 ns). Increasing equilibration times above 70 ps (and thus decreasing data collection times below 100 ps) showed no significant difference.
26. S. C. Colbeck, *J. Cryst. Growth* **72**, 726 (1985). Although temperatures above 253 K were dealt with, no change in behavior below 263 K was reported. The relative surface area of the basal-plane faces was somewhat greater than that of the prism faces below 263 K. Thus, the basal-plane face is expected to be more relevant at 190 K.
27. The thermodynamics of the various configurations have not been investigated. We addressed here only HCl additions to the second bilayer, which we believe are likely made during the barrierless adsorption process. Stable additions to the uppermost bilayer are also possible, as part of bilayer formation or as a result of the replacement of existing waters; however, we believe both of these are activated processes and thus did not consider upper monolayer sites in this first investigation.
28. There were numerically observable second-bilayer effects. For case II, $S_R = 0.70$ and $S_T = 0.70$ for the molecular reactants in monolayer 3, but $S_R = 0.60$ and $S_T = 0.57$ for the CIP products. By contrast, there was no significant change for case I; $S_R = 0.68$ and $S_T = 0.68$ for the molecular reactants in monolayer 3, and $S_R = 0.68$ and $S_T = 0.69$ for the CIP products.
29. We inferred above from experiment (7) that these sites represent the majority of HCl available for reaction on the basal-plane face. For completeness, the remaining HCl atop the surface will need to be examined in the future (along with the prism face and surface defects). After this work was completed, we became aware of the work of S. H. Robertson and D. C. Clary, *Faraday Discuss. Chem. Soc.*, in press. The authors suggest that HCl ionization is energetically favorable from the adsorption site atop the ice surface identified in (14). However, these calculations did not establish that the free energy of the CIP in its equilibrated ice surroundings is lower than the corresponding quantity for the MP.
30. D. R. Hanson and A. R. Ravishankara, *J. Phys. Chem.* **96**, 9441 (1992).
31. L. A. Barrie, in *The Tropospheric Chemistry of Ozone in the Polar Regions*, H. Niki and K. H. Becker, Eds. (Springer-Verlag, New York, 1993), pp. 3–24.
32. R. N. Pribble and T. S. Zwier, *Science* **265**, 75 (1994).
33. If the HCl–H₂O hydrogen bond strength of (14) is doubled (from 4.7 to 9.4 kcal/mol) to account for two hydrogen bonds, the residence time increases to ~30 ms. An alternative estimate of a residence time is ~0.8 ms, based on the experimentally estimated 8 kcal/mol desorption energy of (molecularly adsorbed) α -HCl on HCl · (H₂O)₆ at 140 K, reported by J. D. Graham and J. T. Roberts [*J. Phys. Chem.* **98**, 5974 (1994)]. An HCl with two hydrogen bonds would not be expected to ionize [see (16) and M. J. Packer and D. C. Clary, *J. Phys. Chem.* **99**, 14323 (1995)].
34. M. D. Newton, *J. Chem. Phys.* **67**, 5535 (1977).
35. We thank K. Ando for assistance with the electronic structure calculations and gratefully acknowledge useful conversations with R. Bianco, S. M. George, A. R. Ravishankara, J. T. Roberts, M. A. Tolbert, and V. Vaida. This work was supported in part by a grant from the Petroleum Research Fund, administered by the American Chemical Society, by National Science Foundation grant CHE 93-12267, and by a special Scientific Computing Division grant for supercomputer time from the National Center for Atmospheric Research.

8 November 1995; accepted 22 January 1996

by heterogeneity elsewhere. For the parameterization of the model space by means of local basis functions, we used blocks with lateral dimensions of 1° by 1° within the study region (Fig. 1B) and approximately equal area blocks of 5° by 5° at the equator (Fig. 1C).

From our inversions, we infer that the subducted slab is defined by a laterally continuous region of higher than average *P*-wave velocity in the upper mantle, transition zone, and lower mantle (Fig. 2). In the upper mantle (Fig. 2A), the image of the slab parallels the present-day Sunda arc and the Molucca collision zone. In the mantle transition zone (Fig. 2B), a high-velocity slab is inferred beneath the Java and Banda arcs (note the broadening in map view of the slab beneath the Banda arc) but not beneath Sumatra. A prominent feature in the lower mantle images is the elongated structure of high *P*-wave velocity trending east-west over a distance of ~2500 km from below the northwestern tip of Sumatra to below the Philippines (Fig. 2C). From our global model (15), we infer that this structure forms the easternmost part of a ~10,000-km-long anomaly that extends from beneath southern Asia to the eastern Mediterranean, where it connects to the deep anomaly beneath the Aegean Sea (20). This large-scale structure may be remnant slab of the subducted Izangi Plate that underlaid the Mesozoic Tethys Ocean.

We investigated the reliability of the images with various resolution tests (21). As an example, we discuss the use of a model slab designed specifically for the assessment of the lower mantle slab and the complex structure beneath Sumatra. In the upper mantle, the model slab is characterized by a narrow zone of high seismic velocity along the island arcs (Fig. 2D, inset); in the transition zone, positive velocity anomalies were assigned to the mantle beneath Java and Banda, leaving a gap beneath Sumatra (Fig. 2E, inset); and in the lower mantle, the model slab consists of an east-west-trending high-velocity anomaly (Fig. 2F, inset). From this artificial model, we computed synthetic data using the same path coverage as in the inversion of reported phase data and added random errors. Subsequently, we inverted the synthetic data and compared the output with the known model slab. The result (Fig. 2, D through F) demonstrates that the main features of the model slab are adequately resolved from the noisy data. Locally, uneven sampling produces spurious features in the images. In the mantle region of our interest, the amplitude of this undesirable structure is less than 10% of that of the main structures and is therefore not visible in Fig. 2, D through F. Assuming that the data contain enough structural signal, we conclude from

this and other tests that the sampling by *P*- and *pP*-wave paths is sufficient to map structural features with lateral dimensions of more than 150 and 300 km in the upper and lower mantle, respectively, and that image distortion owing to uneven sampling is too small to invalidate our conclusions based on the large-scale structure.

The complexity of the inferred slab structure is further illustrated by vertical sections across the Sunda and Banda arcs (Fig. 3). Beneath the western end of the curved Banda subduction complex, the dip of the high-velocity anomaly decreases abruptly in the transition zone (Fig. 3A), in agreement with the observed seismicity within the slab (6, 22). Further west, the Indo-Australian Plate dips steeply beneath the Java arc and is only partially outlined by a seismic zone (Fig. 3, B and C). In the seismic gap, between 350 and 500 km in depth, we detected higher than average seismic velocities with small amplitudes. We tested whether this reduced signature of the slab is significant by inverting synthetic, noisy data computed from model slabs that are either continuous or discontinuous across the seismic gap. These inversions indicated that the Java slab is probably continuous and that the amplitude reduction in the seismic gap may be realistic, which may suggest a thinning or “necking”

of the Java slab (23). The Java slab seems to deflect in the uppermost lower mantle, and the continuation of flow to even larger depths is offset to the north (Fig. 3, B and C). The kink in the slab gradually decreases toward the west, and the lower mantle slab is almost vertically below the northwestern tip of Sumatra (Figs. 2C and 3D). The detection of a positive velocity anomaly in the lower mantle beneath Sumatra (Fig. 3D) suggests that the deep part of the slab is detached from the seismogenic slab. Examination of anomaly maps for different depth intervals suggests a northwestward increase of the depth range in which the fast slab is absent because of the decrease of the depth to the leading edge of the upper mantle slab. The precise geometry of the detachment zone cannot, however, be established conclusively from the images.

The three-dimensional shape of the Sunda slab as inferred from Figs. 2 and 3 is summarized in Fig. 4. Assuming that this interpretation is correct, we now discuss a plausible scenario that relates the three-dimensional slab structure—in particular, (i) the slab in the lower mantle, (ii) the kink in the slab, (iii) its lateral variation, and (iv) the slab detachment beneath Sumatra—to the geological history of the arc system.

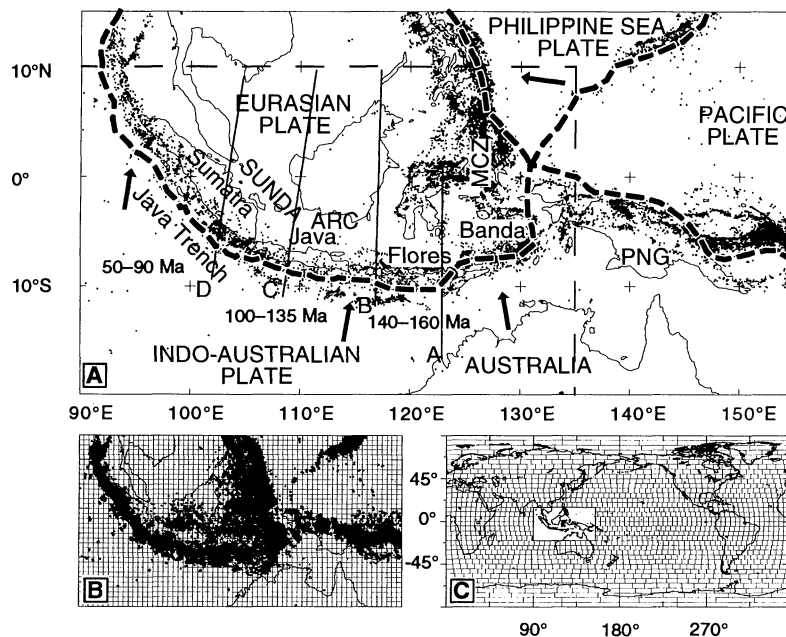


Fig. 1. (A) Seismicity map of the Indonesian region. Solid lines depict the position of cross sections displayed in Fig. 3. Fat dashed lines indicate major plate boundaries after NUVEL-1 by DeMets *et al.* (31). Thin dashed lines indicate the study area. Arrows indicate the direction of plate motion relative to the Eurasian Plate. Small dots depict epicenters of earthquakes used in this study (17). Abbreviations: MCZ, Molucca collision zone; PNG, Papua New Guinea. (B) Surface reflection points of *pP* and *pwP* waves (dots). The *pP* and *pwP* waves initially propagate upward from the source and are reflected at the land-air and water-air interfaces, respectively, to distant receivers. In the absence of seismological stations and shallow events in the back arc regions, depth phases sample mantle structure beneath these regions better than direct *P* waves. The grid of nonoverlapping blocks of horizontal dimension 1° by 1° depicts the parameterization used inside the study region. (C) Global parameterization used outside the volume under study. We used approximately equal area blocks of 5° by 5° at the equator.

The evolutionary history of the large tectonic units in the Indian Ocean region is known from sea-floor spreading isochrons, but the movement of smaller blocks within the complex plate boundary zone is not well constrained. Parts of present-day Indonesia probably rifted from northeastern Gondwana and accreted in Eurasia during the Late Jurassic (24). The time of initiation of northward subduction of Tethyan Ocean floor (Izangi Plate) beneath these allochthonous terranes along the proto-Sunda trench is enigmatic, but arc magmatism (1, 2, 25) and ophiolite emplacement (26) date

back to the Cretaceous. Even allowing for a temporary waning or cessation of subduction in the Late Cretaceous to Early Tertiary, as suggested by the magmatic record (1, 2), several thousands of kilometers of oceanic lithosphere of the Indo-Australian Plate must have been consumed at this margin (4). The observation of a deep slab beneath the Sunda arc is consistent with such a long history of subduction.

Fluid dynamical modeling demonstrated that a kink in the subduction trajectory can occur if the shallow part of the slab moves sideways while the sinking lithospheric slab

encounters resistance against unobstructed penetration into the lower mantle. This resistance can be caused by an increase in viscosity (27, 28), by dynamical effects of the endothermic phase change that coincides with the 660-km seismic discontinuity (28), and by an increase in intrinsic density resulting from compositional layering (29). The kink in the lithospheric slab as inferred

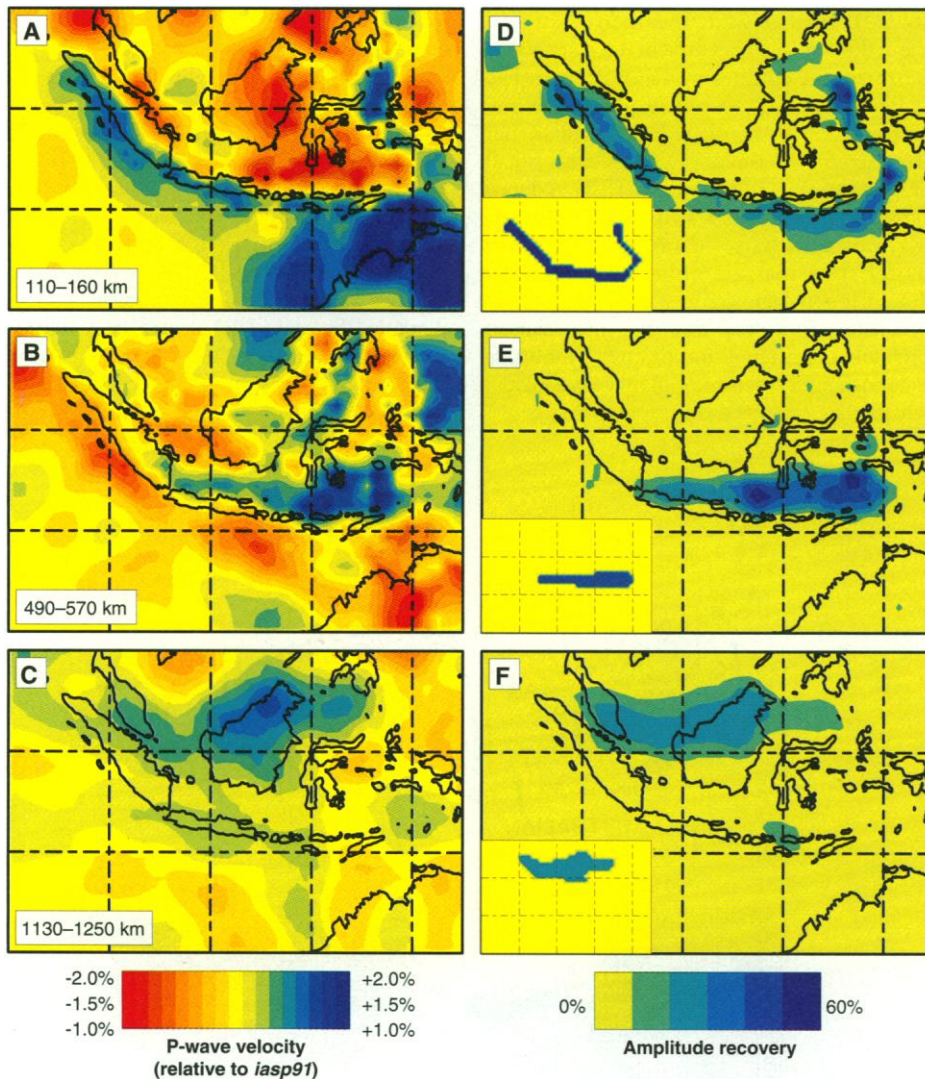


Fig. 2. Layer anomaly maps depicting results of the inversion for the region depicted by thin dashed lines in Fig. 1A. Blue (red) depicts high (low) P -wave velocity. The dashed lines depict parallels and meridians at 10° intervals. (A) Solution representing upper mantle structure. Contour scale is -2 to $+2\%$ relative to *iasp91*. (B) Transition zone (scale: -1.5 to $+1.5\%$). (C) Lower mantle (scale: -1.0 to $+1.0\%$). (D) through (F) Recovery of a slab model designed from the inversion results in (A) through (C) (see inset in lower left hand corner for input at each depth interval). Velocity perturbations in the input model are set to 5, 4, and 3% relative to *iasp91* for the slab in the upper mantle, transition zone, and lower mantle, respectively, and zero elsewhere. Artificial random errors between -1.0 and $+1.0$ s for P and -1.5 and $+1.5$ s for pP were added to the synthetic data. We used an input model with spatial characteristics similar to the slab structure inferred from the data inversion (A through C) to assess the effect of damping (14, 21). For the lower mantle, we applied a slightly larger damping. Amplitude recovery is 60% at best for all depth levels considered; the anomalies in (A) through (C) are underestimated accordingly by at least 40%.

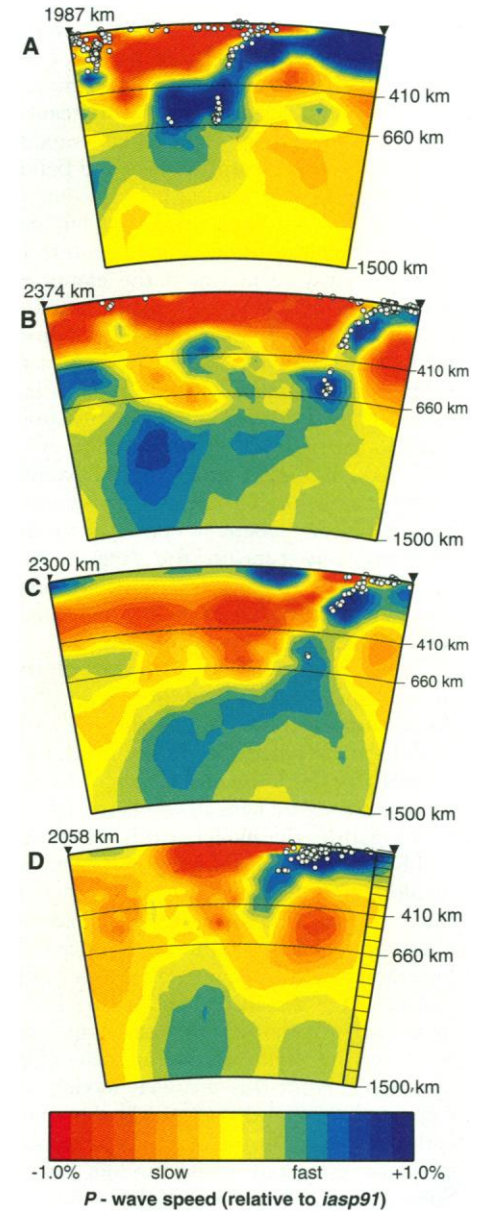


Fig. 3. Vertical cross sections of tomographic images across the Sunda arc. (A) Westernmost Banda arc. (B) East Sunda (between Flores and Java). (C) Central Sunda (Java). (D) West Sunda (Sumatra). Sections are plotted from the back-arc in the north (left) to the fore-arc region in the south (right). Open dots depict earthquake hypocenters of magnitude ≥ 5.5 on the Richter scale, projected from a distance of up to 50 km on both sides of the plane of section. The model parameterization in the radial direction is illustrated at the right side of (D). Notice the necking of the slab across the seismic gap in (B) and (C).

from, for instance, Fig. 3B can be explained by viscosity layering alone but does not conclusively rule out a controlling effect of the phase boundary with a moderately negative Clapeyron slope or a small increase in intrinsic density, provided flux is allowed between the upper and lower mantle.

At first glance, the along strike variation in slab morphology beneath the Sunda arc appears similar to that beneath the Tonga-Kermadec arc [compare, for instance, Fig. 3, B through D, with figure 3 of (13)], but we argue that the deep Sunda slab evolved differently. Kinks in the subduction trajectory beneath southwestern Pacific island arcs were explained by retrograde motion, or roll back, of the slabs in a dynamically self-consistent way, causing oceanward trench migration and concurrent back arc spreading. Lateral variation in the shape of slab was explained by trench rotation accompanying changes in plate motion (12, 13). As a result of the rotation, the Tonga trench has remained orthogonal to the direction of subduction. In contrast, the Sumatra trench is oblique to the present-day direction of plate motion, and from the difference in the strike of the high-velocity anomalies in the upper (Fig. 2A) and lower mantle (Fig. 2C), we infer a clockwise rotation of the shallow slab relative to the deep slab. The inference that the strike of the lower mantle slab is consistent with the present-day direction of subduction of the Indo-Australian Plate beneath Eurasia (30, 31) suggests that the rotation cannot be explained by a change in the direction of the relative motion of the major plates. Instead, we postulate that the rotation of Sumatra relative to the deep slab may have been caused by the northward movement of India during the Early Tertiary (3) and the collision of a mid-oceanic ridge complex with the volcanic arcs of western Indonesia (2-4, 32). The resulting escape tectonics in southeastern Asia (2, 3) included clockwise rotation of tectonic units in Indochina and Indonesia and is nicely illustrated by com-

puter reconstructions of plate motions between ~60 and ~6 Ma (4). The northward indentation of India in the west and the southward expansion of the overriding plate in the east may have formed a torque that caused rotation of the Sunda trench. This torque may have been enforced by tensional stresses along the Java trench (Fig. 4) owing to the large negative buoyancy of the old oceanic lithosphere (5), which may have facilitated the oceanward migration of the eastern part of the Sunda arc and, consequently, the kinking of the slab.

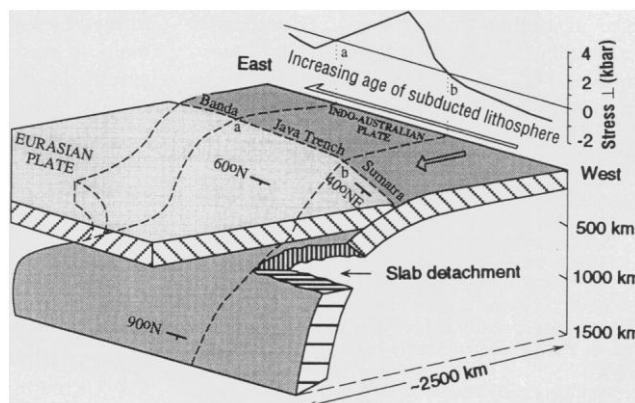
The discussion of the slab detachment beneath Sumatra is still tentative. From finite element modeling, Cloetingh and Wortel (5) inferred a small slab pull for Sumatra and a large increase in tensional stress in the region just east of 105°E, that is, western Java, and the regions of either detachment or continuity of the Sunda slab as inferred from the tomographic images correlate well with the tectonic stress perpendicular to the Sunda arc (Fig. 4). At this stage, we can only speculate on the evolution of the slab detachment. It is possible that the detachment was triggered by the Early Tertiary arrival of the oceanic spreading center at the western Sunda trench. The buoyancy of the young lithosphere and the change to oblique subduction because of the rotation of Sumatra, which reduced flow in the vertical direction (33), may have combined to temporarily cease subduction, while the deep, old slab continued to sink to larger depths. Wortel and Spakman (34) studied the dynamical implications of slab detachment and invoked lateral expansion of a detachment zone to explain the dynamical evolution of the eastern Mediterranean. The observed lateral change in the size of the vertical gap beneath Sumatra may be indicative of a diachronous evolution of the detachment. A southeastward propagation of the detachment would result in a lateral migration of the locus of maximum slab pull, which could have facilitated the rotation of

Sumatra (34, 35). However, the space-time evolution of slab structure below Sumatra is not yet understood in sufficient detail to claim the necessity for lateral propagation of the detachment, and further investigation of this intriguing structural feature is required.

REFERENCES AND NOTES

1. J. A. Katili, *Tectonophysics* **26**, 165 (1975).
2. W. Hamilton, *U.S. Geol. Surv. Prof. Pap.* 1078 (1979), pp. 37 and 81-83; in *Island Arcs, Deep Sea Trenches, and Back-Arc Basins*, M. Talwani and W. Pitman III, Eds. (American Geophysical Union, Washington, DC, 1981), pp. 15-31.
3. P. Molnar and P. Tapponnier, *Science* **189**, 419 (1975); P. Tapponnier and P. Molnar, *Nature* **264**, 319 (1976); P. Patriat and J. Achache, *ibid.* **311**, 615 (1984).
4. C. R. Scotese, L. M. Gahagan, R. L. Larson, *Tectonophysics* **155**, 27 (1988). Solutions of these computer reconstructions are, however, not unique.
5. S. A. P. L. Cloetingh and M. J. R. Wortel, *ibid.* **132**, 49 (1986).
6. B. Isacks and P. Molnar, *Rev. Geophys. Space Phys.* **9**, 103 (1971).
7. K. R. Newcomb and W. R. McCann, *J. Geophys. Res.* **92**, 421 (1987).
8. M. J. R. Wortel and N. J. Vlaar, *Pure Appl. Geophys.* **128**, 625 (1988).
9. S. Kirby, S. Stein, E. Okal, D. Rubie, in preparation.
10. Y. Fukao, M. Obayashi, H. Inoue, M. Nenbai, *J. Geophys. Res.* **97**, 4809 (1992).
11. N. T. Puspito, Y. Yamanaka, T. Miyatake, K. Shimazaki, K. Hirahara, *Tectonophysics* **220**, 175 (1992).
12. R. D. van der Hilst, E. R. Engdahl, W. Spakman, G. Nolet, *Nature* **353**, 37 (1991); R. D. van der Hilst and T. Seno, *Earth Planet. Sci. Lett.* **120**, 395 (1993).
13. R. D. van der Hilst, *Nature* **374**, 154 (1995).
14. The data were inverted for variations in seismic velocity and their effects on hypocenter location [W. Spakman and G. Nolet, in *Mathematical Geophysics*, N. J. Vlaar et al., Eds. (Reidel, Dordrecht, 1988), pp. 155-188; R. D. van der Hilst and E. R. Engdahl, *Phys. Earth Planet. Inter.* **75**, 39 (1992); R. D. van der Hilst, E. R. Engdahl, W. Spakman, *Geophys. J. Int.* **115**, 264 (1993)]. We used the LSQR algorithm [C. C. Paige and M. A. Saunders, *ACM Trans. Math. Software* **8**, 43 (1982); *ibid.*, p. 195; G. Nolet, *J. Comput. Phys.* **61**, 463 (1985)] to solve the large system of equations. The inversion was linearized around the radially stratified *iasp91* reference velocity model (16). Smooth models of slab structure were produced by forcing the solution to the reference values in areas of poor resolution (norm damping) and by minimizing differences in velocity values in neighboring blocks (gradient damping) [G. Nolet, in *Seismic Tomography*, G. Nolet, Ed. (Reidel, Dordrecht, 1987), pp. 1-23]. As a result of the damping, the amplitudes of the velocity variations were underestimated in most parts of the model space, and short wavelength variations were suppressed.
15. The inversion results for mantle structure beneath the entire Indonesian region, as well as the results of the global imaging, will be published elsewhere.
16. B. L. N. Kennett and E. R. Engdahl, *Geophys. J. Int.* **105**, 848 (1991).
17. A procedure that uses an improved global travel-time model, *ak135* [B. L. N. Kennett, E. R. Engdahl, R. Buland, *Geophys. J. Int.* **122**, 108 (1995)], which for mantle *P* waves is virtually identical to *iasp91* (16), and the arrival times of first-arriving regional and teleseismic *P* phases, regional *S* phases, depth phases (*pP*, *pwP*, and *sP*), and the *PKPdf* branch were used to relocate all teleseismically well-constrained earthquakes that occurred between 1964 and June 1994. For the data processing, corrections are applied for Earth ellipticity, topography, bathymetry (at bounce points), and average upper mantle station effects (within 5° by 5° patches). Quality filters for each event include at least 10 reports, azimuthal

Fig. 4. Cartoon summarizing our interpretation of the images of inferred slab structure beneath the Sunda and western Banda arcs. The shallow slab dips in a northeast direction at an angle of ~40° below Sumatra and in a north direction at an angle of ~60° below Java; the deep slab sinks almost vertically into the lower mantle. The tectonic stress perpendicular to the trench as derived by Cloetingh and Wortel (5) is also displayed. Positive and negative stress are associated with tension and compression, respectively.



coverage of more than 180° at teleseismic stations, and standard errors of less than 35 km in location and 15 km in depth. This procedure (E. R. Engdahl, R. D. van der Hilst, R. Buland, in preparation) ensures that depth errors and the mapping of source heterogeneity into mislocation are minimized, thereby creating a powerful uncontaminated database of P , pP , and pwP residuals for use in tomographic imaging.

18. R. D. van der Hilst, B. L. N. Kennett, D. Christie, J. Grant, *Trans. Am. Geophys. Union* **75**, 177 (1994).
19. For stations outside the study area, we combined all ray paths from earthquakes in a particular source region to closely spaced stations elsewhere into a single ray, commonly referred to as the summary ray, to reduce the uneven sampling of mantle structure by ray paths, the dimension of the matrices involved in the inversions (and thus computer memory requirements), and the computer time for ray tracing. The datum (residual time) assigned to the summary ray was the median of all data considered for that summary ray. The number of rays that contributed to the summary ray was not restricted. For stations inside the study area, however, we used individual rays to optimize the sampling.
20. W. Spakman, S. van der Lee, R. van der Hilst, *Phys. Earth Planet. Inter.* **79**, 3 (1993).
21. We inverted data from different time periods and from earthquakes in different depth intervals to test the robustness of structural information in the images. In addition, test inversions were conducted with synthetic data (with and without simulated data errors) computed from the ray distribution as in the real data inversion from isolated target anomalies, checkerboard patterns, and specifically designed, semirealistic slab models (15). One has to be cautious with the interpretation of the results of such tests because they do not simulate accurately the effect of data errors and source mislocation and because they are conducted with the same theoretical assumptions (for example, linearization and neglect of anisotropy) and approximations (for example, parameterization) as in the inversion of reported phase data. Interpretation is further complicated by the dependence of inferences pertinent to image quality on the spatial characteristics of the input model from which synthetic data were computed [J.-J. Léveque, L. Rivera, G. Wittlinger, *Geophys. J. Int.* **115**, 313 (1993)]. The neglect of the effects of the fast slab on wave velocity and ray path position can result in the overestimation of the thickness of the slab [E. R. Engdahl and D. Gubbins, *J. Geophys. Res.* **92**, 13855 (1987)] but probably does not produce an effect on the large-scale structures discussed here that is significant enough to invalidate our conclusions.
22. R. K. Cardwell and B. L. Isacks, *J. Geophys. Res.* **83**, 2825 (1978); P. Lundgren and D. Giardini, *ibid.* **99**, 15833 (1994).
23. The absence of earthquakes between 350 and 500 km in depth could be caused by the low deviatoric stress in the transition from tensional to compressional stress (6, 8) or to the weakening of the plate by the exothermic phase change from olivine to β spinel at ~410 km [D. C. Rubie, *Nature* **308**, 505 (1984); M. J. R. Wortel, *Geophys. Res. Lett.* **13**, 34 (1986)].
24. M. G. Audley-Charles, P. D. Ballantyne, R. Hall, *Tectonophysics* **155**, 317 (1988), and references therein.
25. E. J. Cobbing, D. I. J. Mallick, P. E. J. Pitfield, L. H. Teoh, *J. Geol. Soc. London* **143**, 537 (1986).
26. C. S. Hutchison, *Geol. Soc. Am. Bull.* **86**, 797 (1975).
27. M. Gurnis and B. H. Hager, *Nature* **335**, 317 (1988); C. Kincaid and P. Olson, *J. Geophys. Res.* **92**, 13832 (1987); R. W. Griffiths, R. Hackney, R. D. van der Hilst, *Earth Planet. Sci. Lett.* **133**, 1 (1995).
28. S. Zhong and M. Gurnis, *Science* **267**, 838 (1995); G. F. Davies, *Earth Planet. Sci. Lett.* **133**, 507 (1995); U. R. Christensen, in preparation.
29. U. R. Christensen and D. Yuen, *J. Geophys. Res.* **89**, 4389 (1984).
30. J. B. Minster and T. H. Jordan, *ibid.* **83**, 5331 (1978).
31. C. DeMets, R. G. Gordon, D. F. Argus, S. Stein, *Geophys. J. Int.* **101**, 425 (1990).
32. C.-S. Liu, J. R. Curran, J. M. McDonald, *Earth Planet. Sci. Lett.* **65**, 331 (1983); T. W. C. Hilde, S. Uyeda, L. Kroenke, *Tectonophysics* **38**, 145 (1977).
33. Oblique subduction below Sumatra is comparable

to the oblique subduction of the Pacific Plate at the western Aleutian trench, for which K. C. Creager and T. M. Boyd [*J. Geophys. Res.* **96**, 2293 (1991)] showed from membrane strain calculations that the particle motion in the shallow slab is essentially subhorizontal.

34. M. J. R. Wortel and W. Spakman, *Proc. K. Ned. Akad. Wet.* **95**, 325 (1992).
35. After initiation of slab detachment, the gravitational force exerted on the detached slab results in an increased slab pull and tensional stress in the hinge area of the adjacent segment of continuous slab, which can lead to shear failure and the lateral propagation of the detachment [also see S. Yoshioka and M. J. R. Wortel, *J. Geophys. Res.* **100**, 20223 (1995); S. Yoshioka, D. A. Yuen, T. B. Larsen, *Island Arc* **4**, 89 (1995)]. As a result, the slab pull is small for the region of detachment, increases abruptly near the

hinge region, and assumes normal values where the deep slab is still attached to the surface plate. The laterally migrating concentration of the tensional forces can also result in more pronounced slab roll back and oceanward trench migration, which has been invoked to explain block rotations in the Mediterranean region. In our case, the hinge region is near the transition from Sumatra to Java, close to 105°E.

36. We gratefully acknowledge J. Weekes for the excellent picking of phase arrivals in the *Skippy* records that were used in this study; B. L. N. Kennett, K. C. Creager, O. Gudmundsson, and anonymous referees for reviews; G. Nolet for providing us with his LSQR inversion code; and E. R. Engdahl for early versions of our hypocenter and phase data set. We thank C. Krayshek for producing the final draft of Fig. 4.

5 September 1995; accepted 29 December 1995

The Majorite-Pyrope + Magnesio-wüstite Assemblage: Constraints on the History of Shock Veins in Chondrites

Ming Chen, Thomas G. Sharp, Ahmed El Goresy,*
Brigitte Wopenka, Xiande Xie

Shock veins in the Sixiangkou (L6) chondrite contain two high-pressure assemblages: (i) majorite-pyrope solid solution plus magnesio-wüstite that crystallized at high pressures and temperatures from a shock-induced silicate melt of bulk Sixiangkou composition and (ii) ringwoodite plus low-calcium majorite that were produced by solid-state transformation of olivine and low-calcium pyroxene. The morphology and chemistry of the majorite-pyrope garnet and the size of the magnesio-wüstite crystals indicate a longer duration at high pressure and temperature than predicted by impact scenarios. This pressure-temperature regime is constrained by the olivine-ringwoodite and orthopyroxene-majorite phase transformations, fusion of the meteorite constituents, and crystallization of majorite-pyrope solid solution plus magnesio-wüstite from that melt under high pressure.

Forsteritic olivine [$Fe/(Fe+Mg) < 0.26$] transforms into the denser polymorphs modified spinel (wadsleyite, β phase) and spinel (ringwoodite, γ phase) in the Earth's transition zone (1–4) and dissociates at pressures $P > 23$ GPa and temperatures $T \geq 1600^\circ\text{C}$ to perovskite plus magnesio-wüstite in the Earth's lower mantle (5). Majorite ($Mg_4Si_4O_{12}$ garnet) is a stable phase in the pressure range 19 to 24 GPa at temperatures between 1700° and 2600°C and transforms to a perovskite-type structure at higher pressures (6). Along with experimental investigations at high pressures and temperatures, mineral assemblages in heavily shocked meteorites can reveal

crucial information about phase transitions and high-pressure minerals (7–9). Unfortunately, our understanding of shock-induced phase transitions and the conditions of high pressure and temperature in shocked meteorites is limited by the fact that shock experiments do not produce such transformations. To understand the pressure and temperature conditions and the durations of shock events in chondrites, one must examine the minerals that crystallize from shock melts at high pressure as well as those formed by solid-state transformation. Shock melts in terrestrial and lunar rocks, for example, do not crystallize high-pressure minerals, whereas shock veins in chondrites do (8, 10). This difference suggests a distinction between the pressure-temperature histories of impact events on chondritic asteroids and those on the Earth and moon.

The heavily shocked Sixiangkou meteorite contains black veins, ranging in width from 0.1 to 2 mm, that consist of two lithologies: (i) mostly unfractured, rounded, large polycrystalline grains of ringwoodite and low-Ca majorite (15 to 300 μm in diameter), plus diaplectic plagioclase glass (10 to 60 μm in diameter), and (ii) a fine-grained matrix

M. Chen, Max-Planck-Institut für Kernphysik, Saupfercheckweg 1, D-69117 Heidelberg, Germany, and Guangzhou Institute of Geochemistry, Academia Sinica, 510640 Guangzhou, China.

T. G. Sharp, Bayerisches Geoinstitut, Universität Bayreuth, D-95440 Bayreuth, Germany.

A. El Goresy, Max-Planck-Institut für Kernphysik, Saupfercheckweg 1, D-69117 Heidelberg, Germany.

B. Wopenka, Department of Earth and Planetary Sciences, Washington University, St. Louis, MO 63130, USA.

X. Xie, Guangzhou Institute of Geochemistry, Academia Sinica, 510640 Guangzhou, China.

*To whom correspondence should be addressed.